RESEARCH ARTICLE SUMMARY

IMMUNOLOGY

Induction of CD4 T cell memory by local cellular collectivity

Michal Polonsky, Jacob Rimer, Amos Kern-Perets, Irina Zaretsky, Stav Miller, Chamutal Bornstein, Eyal David, Naama Meira Kopelman, Gil Stelzer, Ziv Porat, Benjamin Chain*, Nir Friedman*

INTRODUCTION: Fate decisions play a central role in the operation of the vertebrate immune system. The establishment of efficient acquired immune responses depends on the differentiation of naïve T cells into various effector and memory cell types upon recognition of a cognate antigen, and on the appropriate balance between these populations. A number of studies have shown that the balance between effector and central memory T cells is shifted in favor of the latter when more T cells participate in the response. This observation has the hallmarks of quorum sensing, the ability of cells to respond to their population density. However, the mechanisms driving this behavior in T cells remain elusive.

RATIONALE: We observed increased differentiation of progenitor central memory T cells (pTCMs) at high cell densities both in vivo and in vitro. However, activated T cells rapidly form dense dynamic clusters, precluding the distinction between the effects of local interactions within cell clusters from global, long-range interactions through soluble factors. To overcome these difficulties, we used live-cell imaging to track the proliferation and differentiation of cells cultured in microwell arrays. This microculture system provides precise control and monitoring of the number of interacting T cells and their state after T cell activation. Continuously tracking differentiation and proliferation enabled us to investigate the mechanisms of cellular collectivity and its influence on memory differentiation.

RESULTS: We first validated that the pTCM cells formed early in our cultures show the markings of established central memory T cells using RNA sequencing and in vivo experiments. Then, with our microwell system, we showed that the rate of differentiation of pTCM cells is determined by the number of cells within individual microwells and sharply increases above a threshold number of locally interacting cells. Further analysis showed that cells follow a universal differentiation trajectory, whereby their differentiation rate is continuously modulated by the instantaneous number of interacting cells, rather than simply by the number of cells present initially within each microwell, or by the number of cell divisions. A combination of experimental manipulation and computational simulations showed that the observed collectivity involved increased sensitivity of clustered T cells to the cytokines interleukin-2 (IL-2) and IL-6, orthogonal to their effect on cell proliferation.

CONCLUSION: By systematically analyzing the role of intercellular interactions in a synthetic microenvironment, we showed that local T cell density could modulate the balance between central memory and effector cells independent of further potential influence by antigen-presenting cells or T cell receptor signaling strength. This cellular collectivity is a continuous process and is not determined by the number of cell divisions, but rather by the number of locally interacting cells at any given time. Local collectivity can influence the diversity and magnitude of immune memory, by modulating interactions between T cell clones during their priming in response to antigens. Understanding the rules of T cell social behavior will be important to learn how to manipulate the immune system for therapeutic or prophylactic goals. ■

ON OUR WEBSITE

Read the full article at http://dx.doi.org/10.1126/science.aaj1853

The list of author affiliations is available in the full article online.
*Corresponding author. Email: b.chain@ucl.ac.uk (B.C.); nir.friedman@weizmann.ac.il (N.F.)
Cite this article as M. Polonsky *et al.*, *Science* **360**, eaaj1853 (2018). DOI: 10.1126/science.aaj1853

Collective local interactions enhance CD4$^+$ memory T cell differentiation. The effects of intercellular interactions on T cell memory formation were studied in microwell arrays, each well holding a different number of locally interacting cells. Proliferation and differentiation were evaluated by using time-lapse movies. Differentiation into memory precursors sharply increased above a threshold number of interacting cells. This was modulated by increased sensitivity of the interacting cells to the cytokines IL-2 and IL-6.

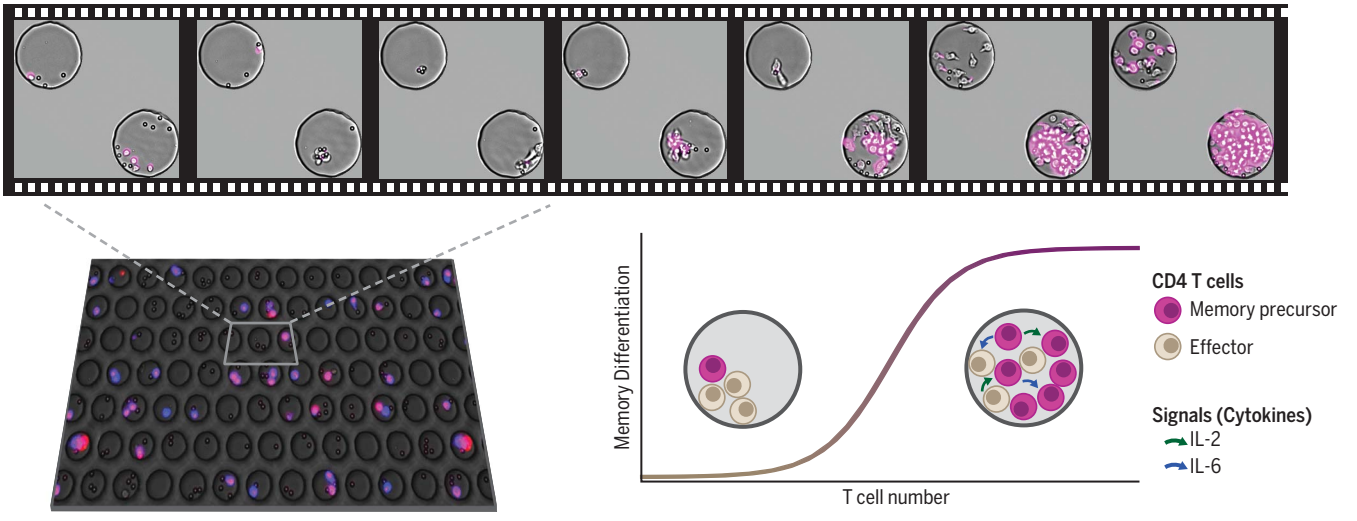

FIGURE COURTESY OF TAL BIGDARI/DIVISION OF RESEARCH SERVICES, WEIZMANN INSTITUTE OF SCIENCE

RESEARCH ARTICLE

IMMUNOLOGY

Induction of CD4 T cell memory by local cellular collectivity

Michal Polonsky[1], Jacob Rimer[1], Amos Kern-Perets[1], Irina Zaretsky[1], Stav Miller[1], Chamutal Bornstein[1], Eyal David[1], Naama Meira Kopelman[2]*, Gil Stelzer[2], Ziv Porat[2], Benjamin Chain[3]†, Nir Friedman[1]†

Cell differentiation is directed by signals driving progenitors into specialized cell types. This process can involve collective decision-making, when differentiating cells determine their lineage choice by interacting with each other. We used live-cell imaging in microwell arrays to study collective processes affecting differentiation of naïve CD4$^+$ T cells into memory precursors. We found that differentiation of precursor memory T cells sharply increases above a threshold number of locally interacting cells. These homotypic interactions involve the cytokines interleukin-2 (IL-2) and IL-6, which affect memory differentiation orthogonal to their effect on proliferation and survival. Mathematical modeling suggests that the differentiation rate is continuously modulated by the instantaneous number of locally interacting cells. This cellular collectivity can prioritize allocation of immune memory to stronger responses.

Upon recognition of a cognate antigen, naïve T cells expand and differentiate into various effector and memory cell types. The establishment of efficient acquired immune responses depends on an adequate balance between these cellular populations. Various models have been proposed to describe the mechanisms that drive T cell specialization, including cell-autonomous stochastic processes (*1*–*3*), deterministic differentiation in response to external signals (*4*, *5*), and asymmetric cell division (*5*–*7*).

T cell number influences memory CD4$^+$ T formation in vivo and in vitro

A number of studies have shown that the function and phenotype of CD8$^+$ T cells that expand in vivo in response to antigen stimulation depends on the number of responding T cells (*8*–*10*). Specifically, central memory T cell (TCM) differentiation is enhanced when a larger number of T cells participate in the response. We observed a similar dependency on cell number in early CD4$^+$ T cell differentiation into CD44$^+$CD62L$^+$ cells (hereafter referred to as progenitor central memory T cells, pTCMs) in vivo, as soon as 5 days after the vaccination of mice with a cognate antigen (Fig. 1, A and B).

T cells differentiate in a complex environment in vivo, interacting with several cell types over time. Thus, we asked whether a dependence on precursor numbers can be observed in a minimal ex vivo system, in which cellular composition and concentration, and cell-cell interactions, can be manipulated and monitored more easily. We isolated naïve splenic CD4$^+$ T cells and cultured them at increasing concentrations in vitro. These T cells were activated either by ovalbumin (OVA) peptide presented by dendritic cells (Fig. 1C, top), by microbeads coated with antibodies against CD3 and CD28 (anti-CD3 + anti-CD28) (Fig. 1C, bottom, and fig. S1, A to C), or by phorbol myristate acetate (PMA) + ionomycin (fig. S1D). Cell state was evaluated by using flow cytometry at different time points. Regardless of cell density and the mode of stimulation, the expression of CD62L decreased to its lowest level 24 hours after activation and then increased in a density-dependent manner (fig. S1B). Increasing the cell density resulted in an increased fraction of pTCMs in response to all activation regimes (Fig. 1C, fig. S1, and table S1). The maximal fraction of pTCMs was different for the various stimulations used, potentially reflecting differences in strength of activation, which have been shown to influence T cell differentiation (*11*). A dependency on cell density was not observed for the activation markers CD69 and interleukin-2 receptor alpha (IL2Ra) (fig. S1, B and C, and table S1). Differences in pTCM frequencies were apparent 48 hours after activation and lasted for at least 96 hours (experimental end point, Fig. 1C; fig. S1, B and C).

pTCMs isolated from 72-hour cultures exhibit a gene expression pattern that is characteristic of established central memory T cells and persist over long time periods in vivo

To further characterize the phenotype of early differentiated pTCMs, we sorted CD62L$^-$ and CD62L$^+$ cells after 72 hours of culture. Each sorted group was subjected to genome-wide gene expression analysis by RNA sequencing (RNA-seq). Together with CD62L (*Sell*), the expression of other T cell central memory–related genes such as *Cd27*, *Il7r*, *Ccr7*, and *IL2rb* (*7*, *12*–*16*) was elevated in CD62L$^+$ cells. The expression of transcription factors (TFs) implicated in memory differentiation such as *Klf2*, *Tcf7*, *Bcl6*, *Foxo1*, and *Eomes* (*17*–*22*) was also increased (Fig. 1D). Thus, pTCMs in culture were associated with a transcriptional program that resembles that of mature memory T cells. The early expression of a transcriptional program resembling that of mature TCM cells was recently observed also in CD8$^+$ T cells, 2 to 4 days after in vivo infection (*7*, *23*). CD62L$^-$ cells expressed high levels of the TF *Id2*, which has been associated with the inhibition of memory differentiation (*24*, *25*). These cells also expressed higher levels of cell cycle and apoptosis-related genes (Fig. 1D) such as *Cdkn1a*, *Myc*, and *Casp3* (*26*, *27*), whereas CD62L$^+$ cells expressed higher levels of homeostatic and self-renewal genes such as *Grap2* and *Cd4* (*28*). This differential gene expression is consistent with our observation that CD62L$^+$ cells exhibited a lower rate of proliferation compared with CD62L$^-$ cells in our culture system (fig. S2). Gene ontology (GO) enrichment analysis (Fig. 1E) revealed that CD62L$^-$ cells are enriched for genes related to apoptosis, ribosomal activity, and nucleotide metabolic processes, suggesting increased cell growth as well as cell death for these cells. CD62L$^+$ cells were enriched for genes related to cytokine responses, leukocyte activation, and proliferation. CD62L$^+$ cells were also enriched for genes associated with cell communication and adhesion, consistent with a role for intercellular interactions in modulating pTCM differentiation.

Initial culture densities also influenced the long-term in vivo persistence of adoptively transferred T cells. Cells activated at high density in vitro persisted in vivo and were fourfold more abundant at late time points (>35 days after in vivo transfer) compared with cells precultured at low density (Fig. 1F). Transferred cells expressed large amounts of the memory markers CD62L and CD27 and low amounts of the activation marker KLRG1 (which is high on T effector cells) relative to host cells (fig. S3B). These results suggest the acquisition of an established central memory phenotype after short-term in vitro stimulation at high cell densities.

pTCM formation is induced by local cellular collectivity

The increased differentiation of pTCMs at high cell densities can arise either from global changes in the composition of the culture medium through cytokine secretion by T cells, or by local interactions between activated cells. T cells in culture rapidly form dense dynamic clusters. Cells join and leave the clusters over time, and clusters can join to form larger clusters, or break into smaller ones (*29*). Thus, in conventional cell cultures as well as in vivo, it is difficult to distinguish the effect of local interactions within cell clusters

[1]Department of Immunology, Weizmann Institute of Science, Rehovot, Israel. [2]Life Sciences Core Facilities, Weizmann Institute of Science, Rehovot, Israel. [3]Division of Infection and Immunity, University College London, London, UK.
*Present address: Department of Computer Science, Holon Institute of Technology, Holon, Israel.
†Corresponding author. Email: b.chain@ucl.ac.uk (B.C.); nir.friedman@weizmann.ac.il (N.F.)

from global long-range interactions. To overcome these difficulties, we used a culture system that employs microwell arrays at the bottom of the culture plate (*30*). Naïve T cells were seeded within small deep microwells (diameter = 80 μm, depth = 120 μm) together with microbeads coated with anti-CD3 + anti-CD28 for activation. Cell seeding was random, such that each microwell held a different number of cells at the beginning of the experiment (Fig. 2A and figs. S4 and S5A). We followed the expansion and differentiation of cells within the microwells by live-cell imaging (Fig. 2, A and B). Cells were imaged for 96 hours, and the levels of expression of CD44 and CD62L were measured with live antibody stain (*31*)

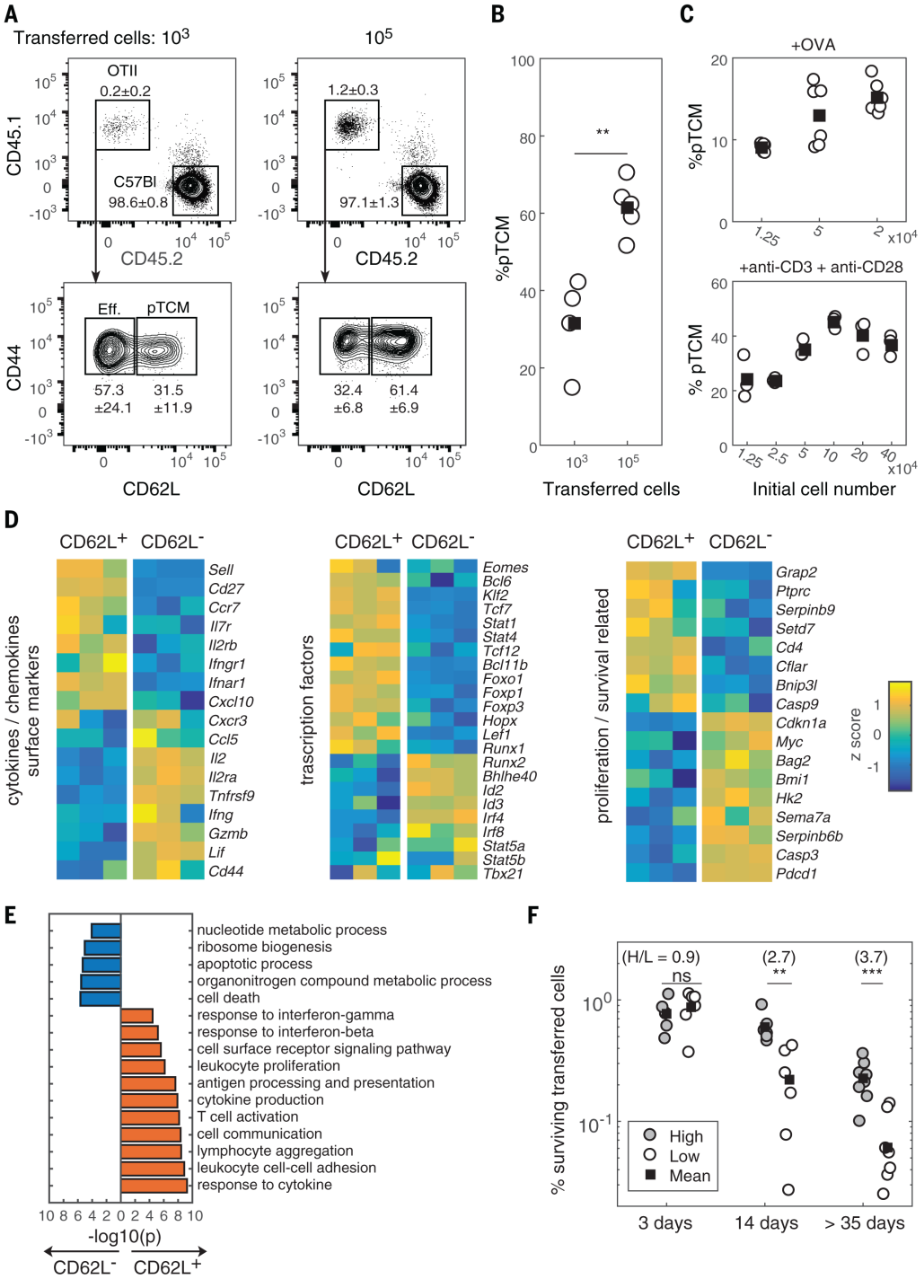

Fig. 1. Differentiation of pTCMs is modulated by T cell number in vivo and in vitro. (**A**) Either 10^3 or 10^5 OT-II TCR transgenic CD4 T cells (CD45.1) were transferred into C57BL/6 recipients (CD45.2), which were then immunized with albumin protein together with an adjuvant (alum). Five days after immunization, the fractions of pTCMs ($CD44^+CD62L^+$) and effector ($CD44^+CD62L^-$) cells were evaluated in the population of transferred cells. Results are from two representative mice out of nine in one experiment. Mean ± SD values are indicated for each population. (**B**) The percentage of pTCMs in mice injected with either 10^3 (n = 4) or 10^5 (n = 5) OT-II cells, 5 days after immunization. Filled squares: mean values. P-value was calculated by a two-tailed Student's t test (**$P < 0.01$). (**C**) The percentage of pTCMs measured at 72 hours in cultures of $CD4^+$ naïve T cells cultured ex vivo at the indicated densities and activated either with OVA-presenting dendritic cells (top, n = 6 samples in one experiment) or with activation microbeads coated with anti-CD3 and anti-CD28 (bottom, n = 3 samples from one representative experiment out of three). Filled squares: mean values. P-values were calculated by using 1-way analysis of variance with $P < 0.01$ in both cases (see table S1). (**D**) The expression levels, measured by RNA-seq, of selected gene transcripts in $CD4^+$ T cells sorted into $CD62L^+$ and $CD62L^-$ populations after 72 hours of culture. Cells were cultured at an initial cell number of 2.5×10^5 cells per well and activated with anti-CD3– and anti-CD28–coated microbeads. (**E**) Gene ontology (GO) enrichment analysis of differentially expressed genes in the $CD62L^+$ and $CD62L^-$ subpopulations. Differentially expressed genes ($P \leq 0.05$, Benjamini–Hochberg correction), with $\log_2$ fold change of ≥0.5 between $CD62L^+$ and $CD62L^-$ samples were chosen for the analysis. Results are from n = 3 repeats. (**F**) Naïve CD45.1 $CD4^+$ T cells were cultured ex vivo for 72 hours in either high (2×10^6 cells/ml) or low (6.25×10^4 cells/ml) initial densities, activated with anti-CD3– and anti-CD28–coated microbeads, and then transferred into CD45.2 recipients (total of 40 mice in two experiments). Spleens were harvested from recipient mice after 3, 14, 35, or 48 days (depending on the experiment). The fraction of donor cells was evaluated out of the total number of $CD4^+CD3^+$ cells in recipient spleens. The recovery of cells precultured in high (filled) or low (empty) concentrations was compared. Fold-change values (High/Low) are indicated in parentheses. Filled squares: mean values. P-values were calculated by a two-tailed Student's t test (**$P < 0.01$, ***$P < 0.001$). ns, not significant.

(Fig. 2, A and B, and movie S1). For each microwell, we extracted time traces of CD44 and CD62L levels, and the area covered by cells, which linearly correlated with cell number (fig. S5B).

The average CD62L and CD44 expression dynamics in the microwells closely resembled those observed by flow cytometry of bulk cultures (fig. S5C). We found that the expression of CD62L, but not of CD44, was dependent on the initial number of T cells in the microwell, N_0. In wells initially containing one or two cells, CD62L was expressed only in a small fraction of the cells at late time points (t = 72 to 96 hours), whereas in microwells initially containing more than seven cells, CD62L was expressed by most cells at these times (Fig. 2, B and C). Moreover, the reexpression of CD62L occurred earlier in microwells with a high initial cell number (Fig. 2B). The level and timing of CD44 expression however, did not depend on the initial cell number (Fig. 2, B and C). Higher cell densities enhanced differentiation toward pTCMs in both microwells and conventional culture. However, the microwell culture established that this effect

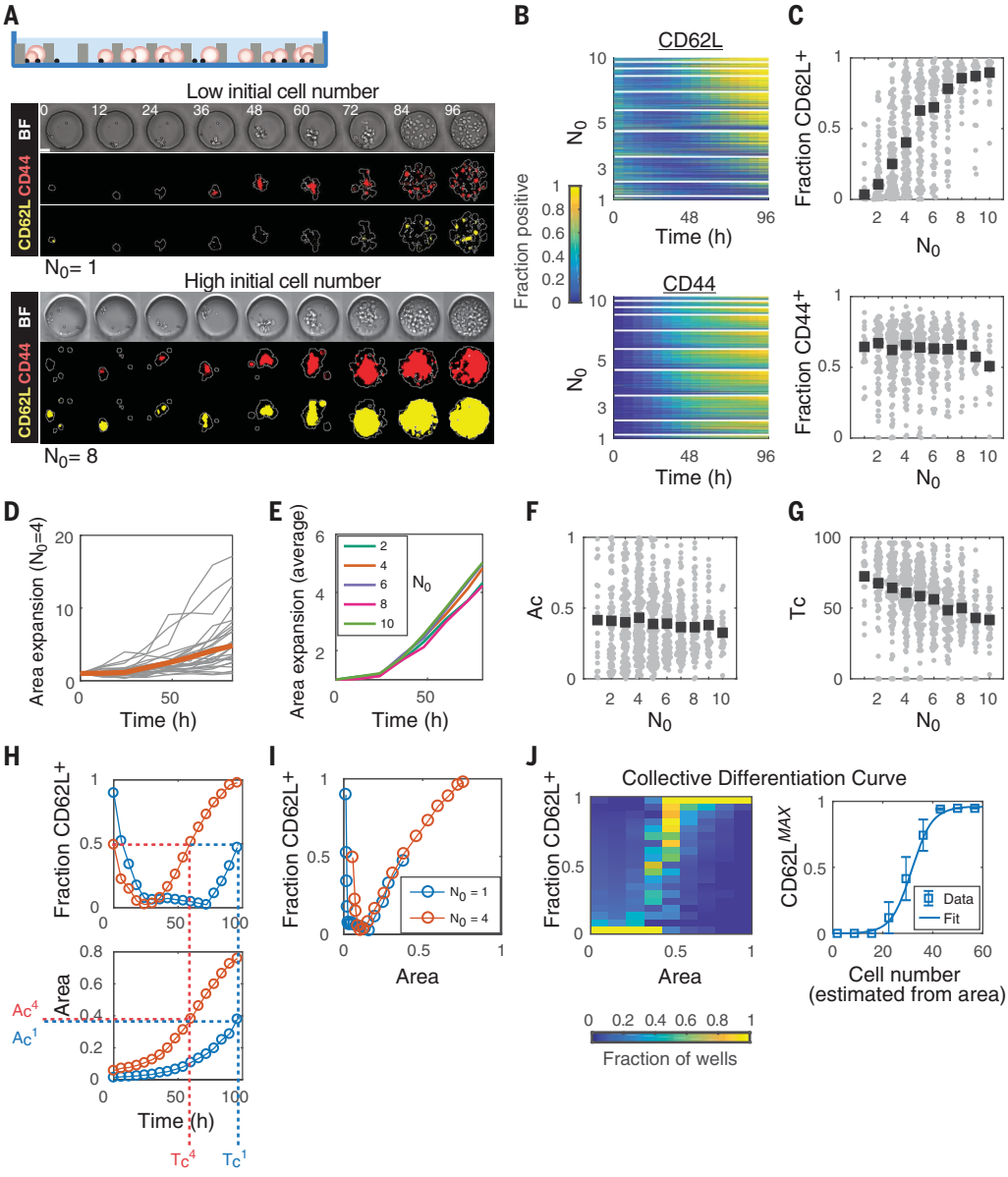

Fig. 2. Induction of CD62L expression depends on local interactions between differentiating T cells. An array of microwells was placed on the bottom of an optical 96-well plate. Naïve CD4 T cells and activation microbeads were seeded such that the microwells randomly received a different initial number of cells (N_0). Cells in different microwells shared the same culture medium. (**A**) Top: Schematic of the experiment, showing the microwell array in side view. T cells and activation microbeads (black dots) are shown. Representative image strips show microwells with N_0 = 1 (top three rows) and N_0 = 8 (bottom three rows). Cells were imaged for 96 hours with bright-field illumination (BF) and two fluorescent channels (CD44, red; CD62L, yellow). Numbers on top show time in hours. Scale bar, 20 μm. (**B**) Time traces of all microwells in one representative experiment out of three (n = 674 microwells) showing the fraction of CD62L$^+$ (top) and CD44$^+$ (bottom) in each microwell over 96 hours. Microwells are grouped by N_0 ($1 \le N_0 \le 10$ initial cells). The color code represents the fraction of positive cells in each microwell. (**C**) Fraction of CD62L$^+$ (top) and CD44$^+$ (bottom) cells after 72 hours of culture, plotted versus N_0. Each gray dot represents one microwell; black squares represent median values. Data are from the same experiment as in (B). (**D**) Representative traces of the area covered by cells, from microwells starting with N_0 = 4 cells. The average trace is depicted in color. All traces are normalized by their initial area. (**E**) Average area traces for microwells starting with different N_0 values. Each trace is normalized by its initial cell area. Data are combined from three experiments (n = 1734 microwells). (**F**) The critical area (A_c), defined as the area in which 50% of the cells are differentiated (CD62L$^+$), plotted versus N_0 for all microwells in three experiments as in (E). (**G**) Critical time (T_c), defined as the time in which 50% of the cells have differentiated, plotted versus N_0 as in (F). (**H**) Traces of two representative microwells starting with one (blue) or four (red) initial cells. Top: fraction of CD62L$^+$ over time; bottom: cell area over time. T_c and A_c are indicated by the dotted lines. (**I**) Fraction of CD62L$^+$ plotted as a function of cell area for the two microwells shown in (H). (**J**) Derivation of the collective differentiation curve (CDC). Left: The frequency distribution of all microwells from all time points in one representative experiment plotted on the area-CD62L$^+$ plane. Right: The CDC is defined by the maxima of the heatmap on the left, binned by cell area. Data for CDC derivation were averaged over eight individual experiments (blue squares). Error bars show SEM. The obtained CDC was fitted with a logistic curve (line) of the form $F(N) = M/\left(1 - e^{(-r(N-N_c))}\right)$; R^2 = 0.99.

was local and was restricted to cells within individual microwells. Indeed, cells in neighboring microwells, which share culture medium, can have different differentiation outcomes based on their initial cell number, despite their proximity (fig. S4). CD62L expression did not depend on the number of activating microbeads (fig. S5D and table S1), precluding competition for a limited amount of stimulatory signals as a cause for enhanced pTCM formation. Thus, the observed collective behavior was driven by short-range interactions that modulated the differentiation of cells within the same microwell.

Collective pTCM differentiation is a continuous process depending on the instantaneous number of interacting T cells

On the basis of these results, we then sought to assess the mechanisms that drive collective differentiation. In particular, we asked whether differentiation depends on the number of cell divisions, on the initial number of interacting cells, or on the varying number of cells that interact (which grows with time because of cell proliferation). This analysis is typically complicated by the fact that the acquisition of a pTCM cell state occurs in parallel with cell proliferation. Thus, it is difficult to distinguish direct mechanisms that affect the differentiation process itself and are not mediated indirectly by their effect on cell proliferation. We found that the number of cell divisions was not a major factor in regulating pTCM formation, as cells cultured in high cell density had higher CD62L expression compared with cells that had the same number of divisions but came from a culture of low cell density (fig. S6). The microwell assay further demonstrated that proliferation did not display the collective characteristic that we observed for CD62L induction. Although the expansion dynamics of cells in individual microwells were highly variable even when starting from the same initial cell number (Fig. 2D), the average proliferation rate was independent of N_0 (Fig. 2E and table S3).

Further insight was gained by examining the relationship between cell area and differentiation within individual microwells. We defined a critical time (T_c) at which 50% of the cells in a microwell were differentiated (CD62L$^+$), and a critical area (A_c), which is the total cell area at T_c (Fig. 2, F to H). When comparing traces of two representative microwells starting with one (blue) or four (red) initial cells, we found that A_c was almost identical in both cases, whereas T_c was much higher in microwells that started with one cell (Fig. 2H). Examining all microwells ($1 \le N_0 \le 10$), we found that the average A_c was independent of initial cell number (Fig. 2F), whereas T_c decreased as initial cell numbers increased (Fig. 2G). Distinctive behavior was observed for CD44, for which T_c was constant, and A_c increased with N_0 (fig. S11A).

When the fraction of CD62L$^+$ cells was plotted as a function of total cell area in individual microwells, we found that both traces collapsed onto the same trajectory (Fig. 2I). This suggests that the level of differentiation did not depend on time since activation or on the extent of cell proliferation, but rather on the instantaneous number of interacting cells. We generalized this observation by projecting all data points of all microwells (regardless of the number of initial cells, time from cell activation, or amount of cell proliferation) onto the area–CD62L plane (Fig. 2J, left). The normalized heatmap showed that cells in individual microwells tended to follow a universal trajectory in the area–CD62L plane. We represented this trajectory with a collective differentiation curve (CDC), which we defined by the local maxima of the heatmap. Thus, the CDC describes the most commonly observed fraction of differentiated cells for a given number of cells in a microwell. The CDC, averaged over eight individual experiments, is plotted in Fig. 2J, right. For further analysis, the CDC was fitted by a logistic function of the form $F(N) = M/\left(1 - e^{(-r(N-N_c))}\right)$, where N is the number of cells in the microwell (which can change with time), N_c is a critical cell number above which differentiation is more efficient, M is the maximal differentiation fraction, and r defines the steepness of the curve.

The existence of a universal differentiation trajectory, which describes all microwells regardless of N_0, was consistent with the above observation that the mean A_c does not depend on N_0, whereas T_c decreases with N_0 (Fig. 2, F and G, and table S1). Additional support for a universal differentiation trajectory came from global gene expression analyses performed at different time

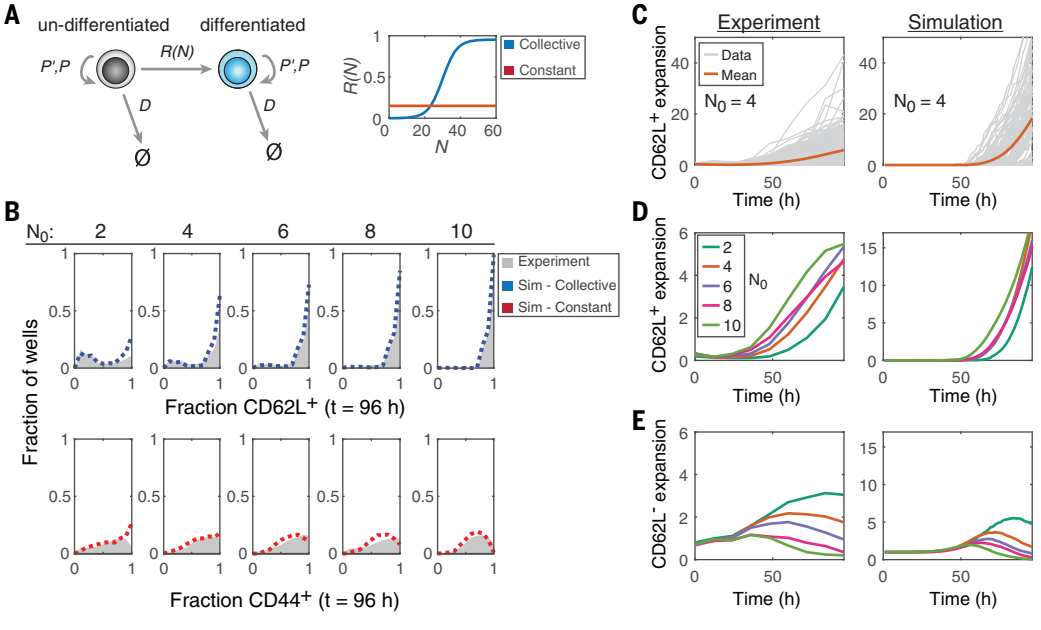

Fig. 3. CD62L expression dynamics can be simulated by assuming collective differentiation. (**A**) A stochastic agent-based model of the differentiation process. Cells can proliferate, differentiate, and die. The proliferation rates (P', first division; P, subsequent divisions) and death rate (D) were experimentally obtained from single-cell data, as detailed in the supplementary text. We assume in the model identical rates for undifferentiated and differentiated cells. The differentiation rate, R, can be either constant ($R_{constant}$, red line) or have a logistic dependence on the number of cells in a microwell ($R_{collective}$, blue curve), $R(N) = M/\left(1 - e^{(-r(N-N_c))}\right)$. (**B**) Distributions of the fraction of CD62L$^+$ (top) and CD44$^+$ (bottom) cells after 96 hours for microwells starting with varying N_0 values. Experimental data (gray) are compared to simulations assuming $R_{constant}$ (red) or $R_{collective}$ (blue). Data are combined from three experiments as in Fig. 2. The parameters used for $R_{collective}$ were obtained from fitting the CDC of Fig. 2J (M = 0.95, r = 0.25, and N_c = 30). $R_{constant}$ = 0.15 gave the best fit to the CD44$^+$ data. (**C**) The relative expansion of CD62L$^+$ cells over time, showing experimentally obtained (left) and simulated (right) traces, of microwells starting with N_0 = 4 cells. The colored trace shows mean values. Data are from the same experiments as in (B). (**D**) The average expansion of CD62L$^+$ cells for experimentally obtained (left) or simulated (right) data, for microwells with different values of N_0. (**E**) Same as in (D), showing average expansion of CD62L$^-$ cells. Traces in (C) to (E) are normalized by their initial value.

points. Cells that grow at low densities followed similar changes in their gene expression pattern but with a delay compared with cells that grow at high cell densities (fig. S7). Together, these findings provide a strong indication for a collective process in which the acquisition of a pTCM state depends on the instantaneous number of interacting cells.

Stochastic simulation recapitulates experimentally observed collective differentiation

To gain a better understanding of the cellular processes giving rise to the observed CDC, we constructed a stochastic computational model simulating a transition from an undifferentiated to a differentiated state (Fig. 3A). The model simulates microwells that initially start with N_0 undifferentiated cells. Cells stochastically proliferate and die at experimentally obtained rates (*32*) (see figs. S8 and S9 and supplementary text for a detailed explanation of model construction). We assumed in the model that division and death rates were identical for differentiated and undifferentiated cells, as delaying the division time of differentiated cells (consistent with the slower division observed for $CD62L^+$ cells; fig. S2) (*33*) did not have a pronounced effect on the simulation outcome (fig. S10). Cells in the model differentiate by some rate R, which can be either constant (R = constant, red line in Fig. 3A) or collective [i.e., dependent on N, the instantaneous number of cells in the microwell (R = collective, blue line in Fig. 3A)]. As we showed that differentiation in our system depended on cell number, we assumed that $R_{\mathrm{collective}}(N)$ had the same functional form as the CDC and used a logistic curve to describe it in the model. The three parameters that describe $R_{\mathrm{collective}}(N)$ (namely M, r, and N_c) were thus extracted from the fit to the experimental CDC (Fig. 2J). We scanned the parameters of the logistic curve and found that the experimentally derived parameters that we used for the simulations were inside a broad optimal region in parameter space (fig. S9, A and B), justifying their use without fitting. This allowed us to run simulations with all model parameters obtained directly from experimental observations.

We then calculated the simulated fraction of differentiated cells at 96 hours for different values of N_0, for both differentiation regimes (constant and collective), and compared them with the measured distributions of $CD62L^+$ and $CD44^+$ cells (Fig. 3B). Simulations assuming collective differentiation fit the $CD62L^+$ data well over all values of N_0 (Fig. 3B, top), much better than simulations of a model based on a constant differentiation rate (fig. S9C). A model assuming a constant differentiation rate, however, fit the $CD44^+$ data (Fig. 3B, bottom). Of note, T_c and A_c obtained by the simulation resembled the experimentally derived values, with the collective and constant differentiation rates showing behavior similar to that of CD62L and CD44, respectively (fig. S11). The stochastic simulation with collective differentiation also captured the well-to-well variability of the experimental data (Fig. 3C), as well as the experimentally observed dynamic changes in the average numbers of both $CD62L^+$ and $CD62L^-$ cells, and their dependence on N_0 (Fig. 3, D and E, and table S3). A model in which cell differentiation depends on the number of neighbors only at the beginning of the experiment, rather than continuously changing with cell number, is less consistent with our data (fig. S11, D and E). We verified experimentally that differentiation remains plastic by transferring T cells into microwells at varying times after their activation in bulk culture and showed that the differentiation outcome depended on the new number of neighbors (fig. S12). Thus, a stochastic model for cell differentiation can describe the experimentally observed collectivity if the differentiation rate R depends on the instantaneous number of interacting cells as described by the logistic CDC, with differentiation markedly increasing above N_c ~30 interacting T cells.

The cytokines IL-2 and IL-6 and the transmembrane protein SLAMF6 modulate collective differentiation

Finally, we sought to identify candidate signaling molecules and pathways that facilitated the observed local collectivity. Short-range interactions between T cells within the same microwell can be mediated by cell-surface ligands and their receptors, as well as by secreted cytokines, which accumulate at high concentrations in the vicinity of the cells and sharply decline with distance (*34*, *35*). Thus, we repeated our microwell array experiments, while adding antibodies to block specific cytokines or surface molecules, or using cells from knockout mouse strains that lacked relevant genes. Out of the several candidate cytokines and genes that we tested, three showed a significant effect on CD62L expression (fig. S13 and table S2). The inhibition of the cytokines interlukin-2 (IL-2) and IL-6 with blocking antibodies reduced CD62L expression after 96 hours of culture (Fig. 4A), whereas the absence of the cell-surface molecule SLAMF6 ($Slamf6^{-/-}$ cells) enhanced its expression (Fig. 4B). We note that blocking IL-2 strongly reduced cell numbers in the microwells at late time points (fig. S14A). To overcome this difficulty, we added IL-6 to increase cell viability (Fig. 4C and fig. S14A) (*29*), without altering CD62L expression (Fig. 4, A and C). Adding back external human IL-2 increased CD62L expression in a concentration-dependent manner (figs. S13 and S14).

Further evidence for the involvement of IL-2 and IL-6 in driving collective differentiation was revealed from investigation of their signaling pathways. We found that in clustering cells, the receptor subunits IL-2Ra and IL-6Rst were nonuniformly distributed on the cell surface and displayed patches that were typically directed toward neighboring cells within the cluster (Fig. 4D and fig. S15, B and C). IL-2 is expressed and secreted by activated T cells at early time points (fig. S15A) (*36*) and is directed toward T-T synapses (*37*). We verified that IL-6 was also produced by T cells in our cultures early after activation (fig. S15A), although we could not infer its localization because of low signal. The polarization of cytokine receptors toward neighboring cells, together with accumulation of cytokines within T cell clusters (*37*), may lead to increased signaling capacity. Supporting this hypothesis, we observed that the phosphorylation of signal transducer and activator of transcription 5 (STAT5) and STAT3 in response to IL-2 or IL-6, respectively, was significantly higher when cells were cultured at high density, thus forming more clusters (Fig. 4E and fig. S16). Finally, we observed that Janus kinase (JAK) inhibitors, which block STAT signaling downstream of IL-2 and IL-6, reduced CD62L expression and pTCM formation, whereas phosphatidylinositol 3-kinase (PI3K) pathway inhibition, which is also activated by IL-2 signaling, did not (Fig. 4F).

IL-2 and IL-6 modulate collective pTCM formation distinctly and orthogonal to their effect on cell proliferation

The CDC derived for each of these perturbations provided a faithful and compact description of the differentiation trajectory, allowing us to assess the net effect on collective cell differentiation, regardless of the effect on cell proliferation and survival. The results recapitulated our previous observations, as blocking IL-2 or IL-6 resulted in reduced $CD62L^{MAX}$ values, whereas in the absence of SLAMF6, $CD62L^{MAX}$ was increased around N_c (Fig. 5A and table S2). The CDC further showed that when IL-2 was blocked but the culture was supplemented with IL-6, CD62L expression remained low even in microwells in which a substantial number of cells had accumulated ($N > N_c$) (Fig. 4C and Fig. 5A, left). Addition of human IL-2 restored the CDC to its unperturbed form in a concentration-dependent manner (fig. S13B and table S2).

The different perturbations can be described by their effect on the parameters of the logistic curve that fits the perturbed CDC. Blocking IL-2 reduced the maximum responsiveness (given by the parameter M), which is consistent with IL-2 regulating the probability of a cell to differentiate at a given number of neighbors (Fig. 5A, left). By contrast, blocking IL-6 only marginally decreased M but shifted the CDC curve to higher cell numbers (Fig. 5A, middle). This is consistent with IL-6 playing a role in decreasing N_c, the critical number of interacting cells that promotes differentiation. The surface molecule SLAMF6 had the opposite effect, as its absence somewhat reduced N_c but did not change M (Fig. 5A, right). We cannot preclude an additional effect of IL-2 also on N_c with the current data. The effects of these perturbations on the CDC can be captured by the stochastic computational model. Changing only the parameter M in $R_{\mathrm{collective}}$ resulted in simulated trajectories that resemble those obtained by blocking IL-2 and also captured the gradual recovery of differentiation that is observed when adding back external IL-2 (Fig. 5B, left, and Fig. 5C, bottom). Simulating reduced proliferation (which is caused by IL-2 blockade) cannot describe the experimentally observed distributions

or the CDC if M is unchanged (Fig. 5, C and D). The experimentally observed behavior for anti–IL-6 and SLAMF6 knockout conditions can be described by changing the parameter N_c in the model (Fig. 5B, middle and right panels). These results demonstrate that the three factors affect collective CD62L expression, orthogonal to their effect on cell proliferation and survival: IL-2 regulates the maximal differentiation rate, whereas IL-6 and SLAMF6 tune the critical number of cells required for differentiation.

Discussion

In this work, we systematically analyzed the role that intercellular interactions between CD4 T cells play in central T cell memory formation. By activating T cells in a synthetic microenvironment, we showed that local cell density can modulate the balance between $CD62L^+$ and $CD62L^-$ cells, independent of further potential influence by antigen-presenting cells or T cell receptor (TCR) signaling strength. Using this system, we could determine that differentiation into memory precursors is most efficient at $N > \sim 30$ interacting cells and that this collective property depends on the instantaneous number of interacting cells, rather than on the number of division cycles the cells undergo.

The signals that direct the development of T cell memory have been studied extensively, and several models of T cell diversification have been suggested (*11*, *38*). Hence, TCR stimulation strength (*39*) and duration (*40*), as well as signaling by various cytokines (*11*), have been shown to modulate the generation and maintenance of memory T cells. Our results support the notion that local, short-range interactions between T cells early after TCR stimulation serve as another potent modulator of memory induction. Depending on the experimental model, local collectivity may influence differentiation to memory or effector phenotypes, depending on the number of precursor cells that participate in the response and their extent of proliferation.

Our findings further suggest that the cytokines IL-2 and IL-6, which are expressed by T cells just a few hours after TCR stimulation, are mediators of local collectivity. The surface protein SLAMF6 also affected collective memory formation, although to a lower extent. Both IL-2 (*41*) and IL-6 (*42*) have been previously shown

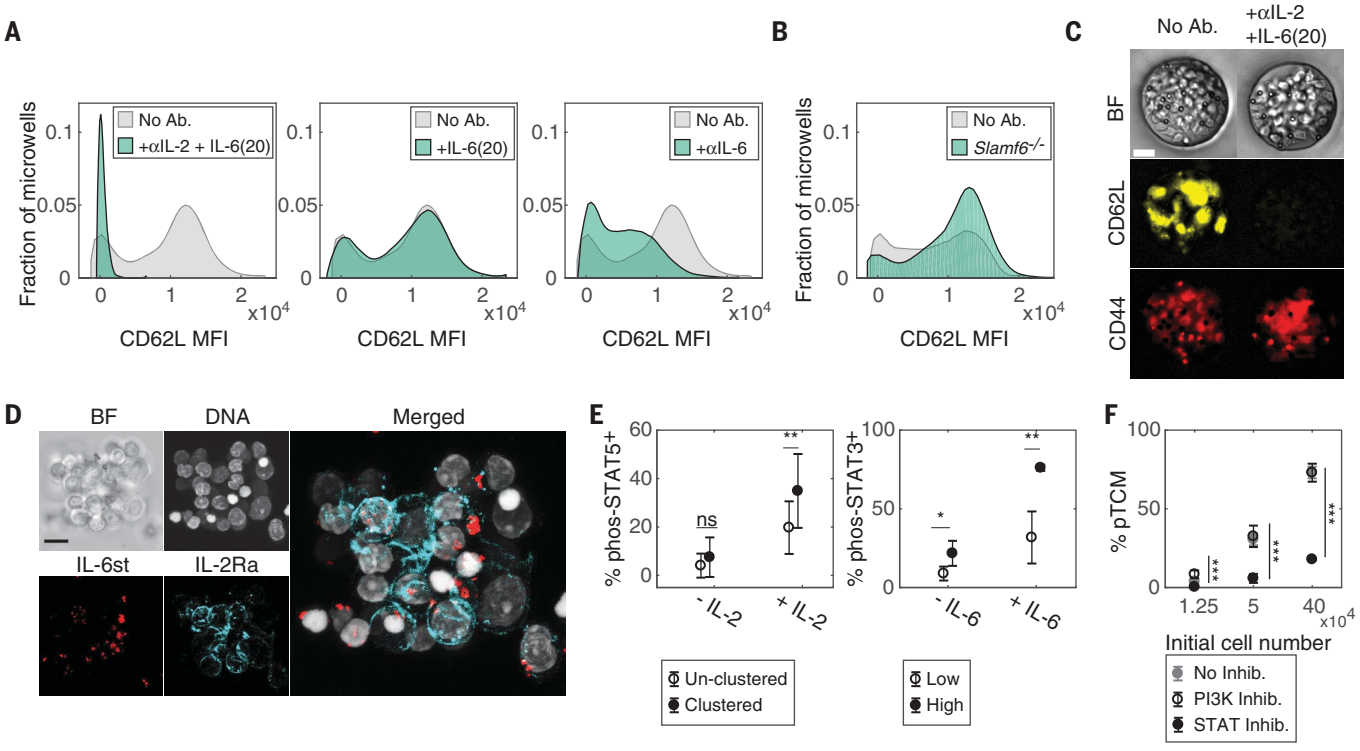

Fig. 4. IL-2, IL-6, and SLAMF6 modulate CD62L expression. (**A** and **B**) Histograms showing the mean expression levels of CD62L at t = 96 hours [given as mean fluorescent intensity (MFI)] in all microwells from two independent experiments, comparing different perturbations (shaded in green) to the control ("No Ab.," shaded in gray). (A) Left: microwells supplemented with 10 μg/ml of anti–IL-2, together with 20 μg/ml of IL-6, which was added to increase cell viability ["+αIL-2 + IL-6(20)," n = 789]. Middle: microwells supplemented with 20 ng/ml of IL-6 ["+IL-6(20)," n = 863]. Right: microwells supplemented with 10 μg/ml anti-IL6 ["+αIL-6," n = 1605]. All three plots show the control sample from the same experiment (n = 812). (B) MFI of microwells harboring *Slamf6*$^{-/-}$ cells (n = 686) compared to control cells (n = 645). (**C**) Representative images of control microwells ("No Ab.") or microwells treated with anti–IL-2 (10 μg/ml) supplemented with IL-6 (20 ng/ml). Images were taken at t = 54 hours of culture. Images show bright-field illumination (BF, top), CD62L (middle), and CD44 (bottom). Scale bar, 20 μm. (**D**) Confocal images of a T cell cluster after 24 hours of activation by using PMA + ionomycin, showing IL-6 receptor (IL-6st), IL-2Ra (CD25), and nuclei (DNA). Images are maximum projection over the total z stack. Scale bar, 20 μm. (**E**) IL-2 and IL-6 downstream signaling of clustered (filled circles) and unclustered (open circles) cells (for phos-STAT5, see also fig. S16), or for cells cultured in dense (filled circles) or sparse (empty circles) cultures (for phos-STAT3). Percentage of phos-$pSTAT5^+$ cells (left) and phos-$STAT3^+$ cells (right) was measured by flow cytometry after 24 hours of culture followed by a 10-min pulse of 5 ng/ml of IL-2 (left) or 10 ng/ml of IL-6 (right). IL-2 data are pooled from three individual experiments with a total of n = 13 samples for each condition. IL-6 data are from one experiment with n = 4 repeats for each condition. (**F**) Small-molecule inhibition of the JAK-STAT and the PI3K pathways. Cells were cultured at the indicated initial cell numbers with either PI3K (empty circles) or JAK-STAT (black circles) small-molecule inhibitors, or without inhibition (gray circles). The percentage of pTCMs was measured by flow cytometry 72 hours after activation. Data were averaged from n = 3 to 4 wells for each condition, from one representative experiment out of three. In (E) and (F), mean ± SD are shown. P-values were calculated by using a two-tailed Student's t test (*P < 0.05, **P < 0.01, ***P < 0.001). P-values in (F) compare STAT inhibition to the control. ns, not significant.

to promote T cell memory differentiation. We found that IL-2 is required for collective pTCM generation at the early stage of the response (< 3 days). IL-2 may have other effects at later time points—for example, at the peak of in vivo responses (*43*, *44*), or during the contraction phase and maintenance of memory cells (*43*), which, together with other cytokines such as IL-7 and IL-15, can further modulate the long-term magnitude of the memory response. We also provided data that suggest that IL-2 and IL-6 contribute to collectivity in the generation of pTCMs at least in part by increased sensitivity of clustered T cells to IL-2 and IL-6. Notably, IL-6 (*42*), as well as members of the SLAMF family of surface receptors (*45*), have been shown to enhance the IL-2 sensitivity of CD4 T cells. Antibodies blocking the adhesion molecule LFA-1 disrupt T cell clustering and affect memory formation in vivo (*46*), but we did not observe a significant effect in our cultures (fig. S13 and table S2). This may stem from different physical constrains or from interactions of T cells with other cells in vivo, which were lacking in our ex vivo cultures. The formation of T cell memory is a highly complex process, and we expect that other molecular components, not yet identified, may contribute to the phenomenon of density-dependent cellular cooperation that we have described.

We hypothesize that the property of increased memory formation above a threshold number of locally interacting cells can have a functional role, as it may prioritize the allocation of immune memory to insults that result in large responses, while preventing aberrant memory of potentially less relevant small events. Local collectivity can also affect the diversity of immune memory, by tuning interactions between T cell clones of different TCR specificities that interact during priming—for example, through clustering on the same antigen-presenting cell. Understanding the rules of T cell social behavior will be important to learn how to manipulate the immune system for therapeutic or prophylactic goals.

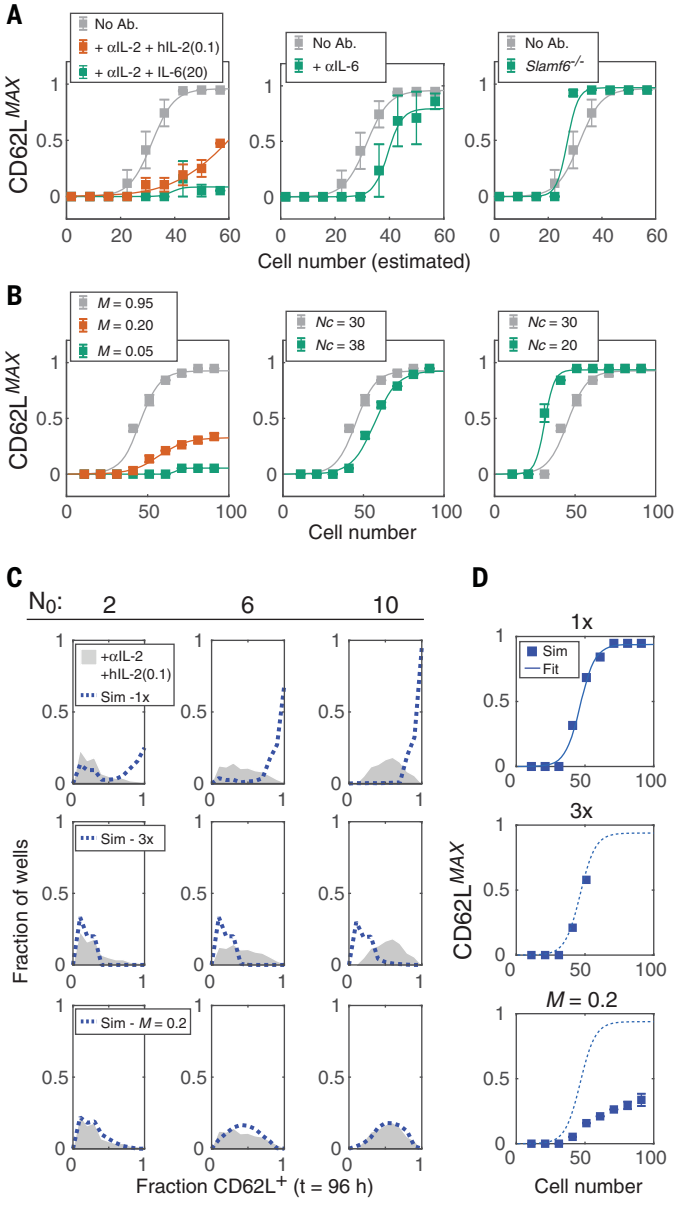

Fig. 5. CDC analysis and stochastic simulations show distinct effects of IL-2 and IL-6 on collective differentiation, orthogonal to their effect on T cell proliferation (**A**) CDC plots for the experimental perturbations shown in Fig. 4, compared to control ("No Ab," gray, averaged over eight individual experiments). The experimental CDCs (squares) were obtained by averaging data from all experiments for each condition (as given below) and were fitted with a logistic function (line). Left: addition of 10 μg/ml of anti–IL-2 supplemented with 0.1 ng/ml human-IL-2 ["+αIL-2 + hIL-2(0.1)," orange, n = 3 experiments] or with 20 ng/ml of IL-6 ["+αIL2 + IL-6 (20)," green, n = 2 experiments]. Middle: addition of anti–IL-6 [10 μg/ml, "αIL-6," green, n = 4 experiments]. Right: *Slamf6*$^{-/-}$ cells [green, n = 2 experiments]. (**B**) CDCs obtained by model simulations using modified $R_{collective}$ parameters. Control CDC (gray) was constructed with a simulation assuming collective differentiation with nominal values as in Fig. 3 (M = 0.95, N_c = 30). Modified parameters that were used are: left: changing the maximal differentiation rate: M = 0.2 (orange) or 0.05 (green); middle: changing the critical cell number: N_c = 38; right: N_c = 20. (**C**) Distributions of the fraction of CD62L$^+$ cells after 96 hours, for microwells starting with varying N_0 values and supplemented with 10 μg/ml of anti-IL-2 and 0.1 ng/ml of hIL-2, as in (A), left. Experimental data (gray) were compared to simulations assuming collective differentiation as in Fig. 3B. As inhibition of IL-2 also inhibits proliferation, the data were compared to a simulation in which the division time of the cells was extended. Top: Division time is unchanged ("1×"); middle: division is three times slower ("3×"); bottom: division time is unchanged and M is reduced (M = 0.2). (**D**) CDC curves of simulation results (squares) for the corresponding conditions in (C). Simulation results with the nominal parameter values (1×, as in Fig. 3) were fitted with a logistic curve, which is shown in all three graphs as a reference.

Materials and methods

Mice

C57BL/6, B6SJL, and TCR-transgenic OT-II mice [harboring ovalbumin (OVA)–specific CD4$^+$ T cells] were housed under specific pathogen-free conditions at the animal facility of Weizmann Institute and were used at 6 to 8 weeks of age. SLAMF6-deficient mice (*Slamf*$^{-/-}$) (*47*) were a donation from the laboratory of I. Shachar from the Weizmann Institute of Science. All animal experiments were performed under protocols approved by the Animal Care and Use Committee of the Weizmann Institute.

Adoptive transfer

For the experiment detailed in Fig. 1A: At day –1, naïve OT-II cells (expressing anti-CD45.1 on a C57BL/6 background) were injected into C57BL/6 recipients. Either 10^3 or 10^5 cells per mouse were injected intravenously (i.v.). On day zero, mice were immunized intraperitoneally (i.p.) with 100 μl of phosphate-buffered saline (PBS) containing 50 μg of albumin protein (Sigma-Aldrich) together with alum as an adjuvant (diluted 1:3, ThermoFisher Scientific). On day 5, total cells were isolated from recipient spleens and stained with APC-Cy7-labeled anti-CD45.1, Alexa Fluor 488-labeled anti-CD45.2, PE-labeled anti-CD3, and PerCP-Cy5.5-labeled anti-CD4 to assess the fraction of donor cells out of recipient CD4$^+$ T cells. Cells were also stained with APC anti-CD62L and PE-Cy7-labeled anti-CD44 to analyze their differentiated state.

For the experiment detailed in Fig. 1F: Naïve CD4$^+$ T cells were isolated from B6SJL mice

(expressing CD45.1) and cultured in low and high initial concentrations (6.25×10^4 and 2×10^6 cells/ml, respectively). Cells were activated using anti-CD3– and anti-CD28–coated microbeads and cultured in six-well plates for 72 hours. At the end of the culture period, dead cells were removed on a Ficoll gradient and either 1×10^6 or 2×10^6 donor cells (depending on the experiment) were injected i.v. into C57BL/6 recipients. At three time points (3, 4, and >35 days), total cells were isolated from recipient spleens. Cells were stained with APC-Cy7-labeled anti-CD45.1, Alexa Fluor 488-labeled anti-CD45.2, PE-labeled anti-CD3, and Pacific Blue-labeled anti-CD4 to assess the fraction of donor cells out of recipient $CD4^+$ T cells. Cells were also stained with APC-labeled anti-CD62L, PE-Cy7-labeled anti-CD44, PerCP-Cy5.5-labeled anti-KLRG1, and Brilliant Violet 510-labeled anti-CD27 to analyze their differentiation state. For antibody specifications, see table S4.

Bulk cell culture

Naïve $CD4^+$ T cells were purified from mice spleens using magnetic microbeads separation ($CD4^+CD62L^+$ MACS T-cell Isolation Kit, Miltenyi Biotec). Unless stated otherwise, cells were cultured in 96-well plates in 200 μl of RPMI. Cells were seeded at varying concentrations indicated in the main text, and activated either with anti-CD3 and anti-CD28-coated microbeads at a 1:1 bead:cell ratio (Dynabeads, Invitrogen) or in the presence of 2 μl/ml cell activation cocktail (PMA + ionomycin, Biolegend). For the experiment presented in Fig. 1C (top), naïve OT-II cells were used and activated using 10 μg/ml OVA peptide (ISQAVHAAHAEINEAGR, InvivoGen) presented by preloaded dendritic cells (1:1 OTII: DC ratio). Cells were cultured in complete RPMI 1640 medium with phenol red, supplemented with 10% (vol/vol) fetal calf serum (FCS), 100 U/ml of penicillin, 100 mg/ml of streptomycin, 2 mM glutamine, 10 mM HEPES, 1 mM sodium pyruvate, and 50 mM β-mercaptoethanol, all from Biological Industries (Beit Haemek, Israel). When cultured for flow cytometry measurements, cells were stained with the proliferation dye eFluor 450 (ebioscience) before the start of culture; after isolation, cells were supplemented with 1 ml of PBS + 1 μl of eFluor-450, incubated for 10 min at 37°C and then washed three times with RPMI.

Extracellular markers flow cytometry sample preparation

Cells were harvested at the different time points indicated in the text (typically at t = 0, 24, 48, and 72 hours), placed in a U-shaped 96-well plate, and washed twice with PBS. The supernatant was aspirated and cells were supplemented with live-dead blue reagent (Invitrogen) diluted 1:1000 in PBS, to a final volume of 20 μl. Samples were then supplemented with 5 μl of antibody mix: PE-Cy7-labeled anti-CD62L, APC-Cy7-labeled anti-CD44, FITC-labeled anti-CD4, PE-labeled anti-CD69, and APC-labeled anti-IL2Ra (0.25 μl/sample for each antibody), to a final volume of 25 μl (for antibody specifications, see table S4). Samples were then incubated in the dark for 30 min at room temperature, washed twice with PBS, and measured using a flow cytometer (LSRII; BD).

Microwell array design and fabrication

Photolithography masks were designed using autoCAD (Autodesk, San Rafael, CA). Molds were designed as an array of several hundred hexagonally spaced microwells, each being 80 μm in diameter and 120 μm in depth. This depth is 12 to 20 times the cell diameter, thus reducing the chance of escape by activated cells. Microwell preparation is described in detail in Zaretsky *et al.* (*30*). Briefly, molds were fabricated using photolithography of negative photoresist on silicon wafers. In a slight alteration from the cited protocol, photoresist spinning was performed twice yielding feature heights of 120 μm. Wafers were exposed to ultraviolet (UV) irradiation on a contact mask aligner using a dark-field mask, hardened, and treated to remove unbound photoresist. PDMS was mixed in 10:1 weight ratio (base:curing agent). One milliliter was then poured onto the template wafer and centrifuged (WS-650S spin processor, Laurell Technologies) for 30 s at 300 rpm followed by 2 min at 1000 rpm. Wafers were then left to stand for 10 min to even the PDMS surface and then baked for 1 hour at 80°C until PDMS was fully cured. After curing, the thin PDMS layer was cut into stripes, peeled, and gently placed on strips of a thick PDMS slice. This thick PDMS was used to help place the thin layer containing the array into a 96-well plate. Small squares (~5 mm by 5 mm) containing the microwell pattern were cut and punched into an optical bottom 96-well plate (Thermo Fisher Scientific, Rochester, NY) using tweezers. As the thin layer adhered strongly to the bottom of the plate, it detached from the thick layer and remained inside the 96-well plate.

Cell loading and culture in microwell arrays

For all microscopy experiments, naïve $CD4^+$ T cells were purified from mice spleens using magnetic microbead negative separation (Naïve $CD4^+$ isolation, StemCell Technologies). Cells were cultured in medium identical to that used for bulk culture, but without phenol red. For all microscopy experiments, activating microbeads were used at a 2:1 bead:cell ratio. To facilitate cell loading into the small-volume microwells and eliminate trapped air bubbles that remained in the microwells due to the hydrophobicity of PDMS, wells were filled with 200 μl of culture medium, and the plate was placed in vacuum for 1 hour followed by 1 min centrifugation at 300*g* to remove residual bubbles. The plate was then left at 4°C overnight. Cells were loaded into the microwell array, followed by loading of the activation microbeads. First, the medium was removed and replaced with 12.5×10^3 primary naïve T cells in 100 μl of culture medium. The plate was centrifuged at 300*g* for 1 min to allow cells to settle. Residual cells were aspirated, and 100 μl of medium containing activation microbeads was loaded into the wells. Beads were left to settle for 5 min after which the medium was aspirated and replaced with 100 μl of fresh tissue culture medium without phenol red as indicated. This seeding procedure gave an average cell number of 4.7 ± 2.6 and average bead number of 8.5 ± 4.5 (fig. S5A). Then, wells were loaded with 100 μl of culture medium supplemented with a combination of FITC-labeled anti-CD44, PE-labeled anti-CD62L, and APC-labeled anti-CD45.2 antibodies in dilutions of $1:5 \times 10^3$, $1:10^4$, and $1:10^4$ respectively. This gave a final culture volume of 200 μl with twice the listed antibody dilution. For antibody specifications, see table S4.

Perturbation in microwells

Whenever antibodies were used, microwells were supplemented with 100 μl of culture medium containing fluorescent antibodies as indicated above, and 100 μl of culture medium containing the blocking antibodies at double the final concentration. Final antibody concentrations were as follows: anti-IL-2 (10 μg/ml), anti-IL-6 (10 μg/ml), anti-IL-15/15R (5 μg/ml), and anti-IL-6Ra (5 μg/ml). IL-6 and recombinant human-IL-2 (both from R&D) were given at final concentrations of 20 ng/ml for IL-6 and 0.1 or 10 ng/ml for human-IL-2.

When anti-LFA-1 and ICAM-1 were used, microwells were precoated with the reagent to interfere with cell-cell adhesion. For anti-LFA-1, microwells were precoated with 20 μg/ml of the antibody in PBS overnight at 4°C. ICAM-1 coating was performed in two steps. First, microwells were coated with protein A to enable correct positioning of the ICAM-1 molecules, and then coated with ICAM-1/Fc chimera protein (R&D): 20 μg/ml of Protein A was diluted in PBS (+calcium +magnesium) supplemented with 1 mM $NaHCO_3$. Seventy microliters of the mix was added to the microwells and incubated for 2 hours at 37°C. Protein A solution was aspirated and replaced with 70 μl of blocking buffer (PBS supplemented with 2% human serum albumin, Calbiochem) followed by a 10 min incubation at room temperature. Finally, ICAM-1 was diluted in blocking buffer to 20 μg/ml, and 70 μl was added to the microwells and incubated overnight at 4°C. Wells were washed with culture medium before cell seeding.

Live cell imaging acquisition

For time-lapse experiments, a Ti-eclipse microscope (Nikon Instruments) was used equipped with an automated stage, incubator, and a closed chamber that allowed for CO_2 flow over the 96-well plate. Cells were imaged using 20×/NA = 0.17 objective (sFlour, Nickon) and monitored using bright-field illumination and three fluorescence channels: FITC, Cy3, and Cy5. Time-lapse movies were collected using the Andor software. Cells were imaged every 2 to 6 hours, depending on the experiment, using an Andor iXon-888 EMCCD camera (1024 × 1024 pixels, 13-μm pixel size).

Confocal microscopy imaging

Naïve CD4 cells were cultured at a concentration of 10^6 cells/ml in 24-well plates, and in the

presence of 2 μl/ml Cell Activation Cocktail (PMA + ionomycin, Biolegend). After 24 hours, paraformaldehyde (PFA, Biolegend) was added directly to the cells to a final concentration of 1.6%, and cells were incubated for 15 min at room temperature in the dark. To keep clusters intact, washing of the cells was performed gently on the culture dish by adding staining buffer (PBS + 4% FCS) and removing it several times. Cells were supplemented with 500 μl of staining buffer with 5 μl of PE-labeled anti-IL-6st and 5 μl of Alexa Fluor 488-labeled anti-IL-2Ra and incubated for 30 min at room temperature in the dark. Cells were washed with PBS and seeded on a six-well plate with a glass bottom. Cells were imaged using Fv3000 laser scanning confocal microscope (Olympus) using PLAPON 60× OSC2 super-corrected objective with 1.4 NA, at a sampling speed of 2 μs/pixel.

PI3K and JAK-STAT inhibition

Naïve $CD4^+$ T cells were cultured in three initial cell numbers as indicated in the text for 72 hours. At the culture start time, small-molecule inhibitors for PI3K (LY-294002, Sigma) and JAK-STAT (AZ-1480, Sellechem) were added to separate cultures at a concentration of 5 μM each. After 72 hours, cells were labeled as described above and measured using flow cytometry.

Pospho-STAT sample preparation

The protocol for phos-STAT measurements was adopted from Feinerman *et al.* (*48*). For phos-STAT5 measurements, naïve CD4 T cells where cultured in 24-well plates at a cell concentration of 1×10^6 cells/ml with activation microbeads (1:1 bead:cell ratio) and in the presence of anti-IL-2 (10 μg/ml) to prevent endogenous IL-2 binding. After 24 hours, unclustered and clustered cells were separated using a 10 μm mesh (PlutiSelect) by performing the following steps: The mesh was washed with culture medium from both sides. Cells were washed and supplemented with 500 μl of fresh medium and (without mixing) passed through the mesh into one well on a 24-well plate; this contained the unclustered cells. The mesh was washed three times with 500 μl of medium, flipped onto a second well, and washed from its other side with 500 μl of medium. This well contained the clustered cells (see fig. S16A for images of clustered and unclustered cells). Each fraction was supplemented with 500 μl of culture medium with 1 μl of live–dead blue reagent and either with or without 5 ng/ml human-IL-2. The culture plate was incubated for 10 min at 37°C and immediately supplemented with PFA (Biolegend) in a final concentration of 1.6%. Cells were incubated in the dark for 15 min at room temperature and then centrifuged at 600*g*. The supernatant was aspirated and replaced with 1 ml of 90% ice-cold methanol followed by a 30 min incubation on ice in the dark. After incubation, cells were washed with staining buffer (PBS + 4% FCS) and supplemented with 90 μl of stain buffer and 10 μl of stain mix containing 5 μl of FITC-labeled anti-pSTAT5 (ebioscience), 1 μl PerCP-Cy5.5-labeled anti-IL-2Ra, 1 μl of PE-labeled anti-CD4, and 3 μl stain buffer. Cells were incubated at room temperature for 30 min in the dark, washed twice with stain buffer, and measured on the flow cytometer (LSRII; BD). For phos-STAT3 measurements, cells were cultured in two initial concentrations: either 1×10^6 or 6.25×10^4 cells/ml. After 24 hours, cells were washed once and supplemented with 200 μl RPMI either with or without 10 ng/ml of IL-6. Cell fixation and staining were performed as described above for phos-STAT5.

Imaging flow cytometry (ImageStream) sample preparation and analysis

Naïve cells were cultured in 24-well plates at a concentration of 10^6 cells/ml with activation microbeads (1:1 bead:cell ratio). After 72 hours of culture, cells were collected into 5 ml tubes and washed with PBS. Supernatant was aspirated and replaced with 100 μl PBS with 10 μM Hoechst 33342 (life technologies) and with Alexa Fluor 488-labeled anti-CD45.2, APC-labeled anti-IL2Ra, and PE-labeled anti-CD3 (1 μl each). Cells were incubated at room temperature in the dark for 30 min, washed once with PBS, transferred to 1.5-ml tubes (Eppendorf), and centrifuged at 400*g*. Supernatant was gently aspirated using a 10-ml syringe, and samples were supplemented with PBS to a final volume of 50 μl. Samples were measured using multispectral Imaging Flow Cytometry (ImageStreamX mark II; Amnis Corp, part of EMD millipore, Seattle, WA). Imaging was performed using 60×/NA = 0.9 lens; the lasers used were 405 nm (120 mW) for Hoechst, 488 nm (100 mW), 561 nm (200 mW), 642 nm (150 mW), and 785 nm (5 mW) for side scatter (SSC) channel imaging. At least 5×10^4 cells were collected from each sample, and data were analyzed using image analysis software (IDEAS 6.2; Amnis Corp). Cells were gated for single cells or doublets using the area and aspect ratio features, and for focused cells using the Gradient RMS feature. $CD3^+CD25^+$ cells were gated, and the relative concentration of the cell–cell synapse was calculated. First, a mask was created to delineate the cell synapse, using the VALLEY mask (rectangular mask that sits between two bright regions, such as between two nuclei. This minimum intensity identifies the intersection between the two objects) dilated for 3 pixels, based on the nuclear Hoechst staining. We calculated the intensity concentration ratio feature (the ratio of the intensity inside the first input mask to the intensity of the union of the two masks); the higher the score, the greater the concentration of intensity inside the first mask. The ratio is mapped to a log scale based on the Valley mask.

RNA sequencing

For $CD62L^{+/-}$ cell sorting (described in Fig. 1, D and E), naïve $CD4^+$ cells were cultured for 48 and 72 hours at a concentration of 2.5×10^5 cells/ml and activated using microbeads as described above. This cell concentration was selected to yield a relatively similar fraction of $CD62L^+$ and $CD62L^-$ cells at the indicated time points. At each time point, $CD4^+CD62L^{+/-}$ cells were sorted into 100 μl of Lysis/Binding buffer (Invitrogen). For comparison between the transcriptome of cells cultured in high and low concentrations (fig. S7), naïve CD4 cells were cultured in 24-well plates (1 ml/well) for 18, 30, 48, and 72 hours at a starting concentration of either 10^6 or 6.25×10^4 cells/ml. At the indicated time points, live $CD4^+$ cells were sorted into 100 μl of Lysis/Binding buffer.

Total RNA was extracted with poly-dT beads (Dynabeads, Invitrogen). We used a variation of the MARS-seq protocol (*49*) developed to produce single-cell RNA-seq libraries. In brief, the protocol consists of special designed primers with unique molecular identifiers (UMI) for accurate molecule counting and a step of linear amplification of the initial mRNA pool, followed by a library construction step. In this way, the diversity of the original pool of messenger RNAs is preserved even if the amount of input RNA is low. Three replicate libraries were prepared for each of the different populations. First, the samples were incubated at 72°C for 3 min and immediately transferred to 4°C. Then, 2 μl of an RT reaction mix [10 mM DTT, 4 mM dNTP, 2.5 U/μl Superscript III RT enzyme in 50 mM Tris-HCl (pH 8.3), 75 mM KCl, and 3 mM $MgCl_2$] were added into each well. The samples were then centrifuged and incubated as follows: 2 min at 42°C, 50 min at 50°C, and 5 min at 85°C. Indexed samples with equivalent amount of cDNA were pooled. The pooled cDNA was converted to double-stranded DNA with a second strand synthesis kit (NEB) in a 20-μl reaction, incubating for 2.5 hours at 16°C. The product was purified with 1.4× volumes of SPRI beads, eluted in 8 μl and in vitro-transcribed (with the beads) at 37°C overnight for linear amplification using the T7 High Yield RNA polymerase IVT kit (NEB). Following IVT, the DNA template was removed with Turbo DNase I (Ambion) 15 min at 37°C and the amplified RNA (aRNA) purified with 1.2× volumes of SPRI beads. RNA was chemically fragmented (median size ~200 nucleotides) by incubating for 3 min at 70°C in Zn^{2+} RNA fragmentation solution (Ambion) and purified with two volumes of SPRI beads. Next, a partial Illumina Read1 sequencing adapter that includes a pool barcode was single strand ligated to the fragmented RNA using a T4 RNA ligase I (New England Biolabs): The RNA (5 μl) was preincubated for 3 min at 70°C with 1 μl of 100 μM ligation adapter. Then, 14 μl of a mix containing 9.5% DMSO, 1 mM ATP, 20% PEG8000, and 1 U/μl T4 ligase in 50 mM Tris HCl (pH7 .5), 10 mM $MgCl_2$, and 1mM DTT was added. The reaction was incubated at 22°C for 2 hours. The ligated product was reverse transcribed using Affinity Script RT enzyme (Agilent) and a primer complementary to the ligated adapter: The reaction was incubated for 2 min at 42°C, 45 min at 50°C and 5 min at 85°C. cDNA was purified with 1.5× volumes of SPRI beads. The library was completed and amplified through a nested polymerase chain reaction (PCR) with 0.5 μM of P5_Rd1 and P7_Rd2 primers and PCR ready mix (Kapa Biosystems): The forward primer contains

the Illumina P5-Read1 sequences and the reverse primer contains the P7-Read2 sequences. The amplified pooled library was purified with 0.7× volumes of SPRI beads to remove primer leftovers. Library concentration was measured by a Qubit fluorometer (Life Technologies), and mean molecule size was determined by TapeStation (Agilent). DNA libraries were sequenced on an Illumina NextSeq 500 with an average of ~1×10^6 aligned reads per sample.

Quantitative PCR

Naïve CD4 T cells were isolated, and 3×10^5 naïve cells were transferred to 1.5 ml tubes (Eppendorf), washed once with PBS, supplemented with 1 ml Tri-reagent (Sigma), and immediately frozen in -80°C, for subsequent RNA extraction (naïve sample). The remaining cells were cultured in 24-well plates at a concentration of 10^6 cells/ml and activated using microbeads. At 8 and 24 hours, cells were detached from the activation microbeads by 5-min incubation in culture medium containing 5 mM EDTA. Then, cells were placed on a magnet for 3 min, and the cell fraction was transferred to 1.5-ml tubes. Cells were washed (450*g* for 10 min) supplemented with 1 ml of tri-reagent and frozen. Total RNA was isolated according to the manufacturer's protocol (Life Technologies). The total RNA was reverse-transcribed into cDNA using M-MLV RT primed with oligo(dT) primers (Promega). Real-time PCR was performed using the Fast SYBR Green master mix in the Quant Studio 5 machine (Applied Biosystems). See table S5 for primer specifications. Primer amplification efficiency and specificity were verified for each set of primers at a final concentration of 250 nM. The determined amounts of cDNA template were 4 ng for *Hprt* and *Il2* and 32 ng for *Il6*. mRNA expression levels of the tested genes relative to *Hprt* were calculated using the ΔΔCt method, with the naïve sample as a reference.

REFERENCES AND NOTES

1. V. R. Buchholz *et al*., Disparate individual fates compose robust CD8$^+$ T cell immunity. *Science* **340**, 630–635 (2013). doi: 10.1126/science.1235454; pmid: 23493420
2. P. D. Hodgkin, M. R. Dowling, K. R. Duffy, Why the immune system takes its chances with randomness. *Nat. Rev. Immunol.* **14**, 711 (2014). doi: 10.1038/nri3734-c1; pmid: 25212742
3. J. M. Marchingo *et al*., T cell signaling. Antigen affinity, costimulation, and cytokine inputs sum linearly to amplify T cell expansion. *Science* **346**, 1123–1127 (2014). doi: 10.1126/science.1260044; pmid: 25430770
4. C. R. Plumlee, B. S. Sheridan, B. B. Cicek, L. Lefrançois, Environmental cues dictate the fate of individual CD8$^+$ T cells responding to infection. *Immunity* **39**, 347–356 (2013). doi: 10.1016/j.immuni.2013.07.014; pmid: 23932571
5. S. L. Reiner, W. C. Adams, Lymphocyte fate specification as a deterministic but highly plastic process. *Nat. Rev. Immunol.* **14**, 699–704 (2014). doi: 10.1038/nri3734; pmid: 25190286
6. J. T. Chang *et al*., Asymmetric T lymphocyte division in the initiation of adaptive immune responses. *Science* **315**, 1687–1691 (2007). doi: 10.1126/science.1139393; pmid: 17332376
7. J. Arsenio *et al*., Early specification of CD8$^+$ T lymphocyte fates during adaptive immunity revealed by single-cell gene-expression analyses. *Nat. Immunol.* **15**, 365–372 (2014). doi: 10.1038/ni.2842; pmid: 24584088
8. A. L. Marzo *et al*., Initial T cell frequency dictates memory CD8$^+$ T cell lineage commitment. *Nat. Immunol.* **6**, 793–799 (2005). doi: 10.1038/ni1227; pmid: 16025119
9. V. P. Badovinac, J. S. Haring, J. T. Harty, Initial T cell receptor transgenic cell precursor frequency dictates critical aspects of the CD8$^+$ T cell response to infection. *Immunity* **26**, 827–841 (2007). doi: 10.1016/j.immuni.2007.04.013; pmid: 17555991
10. J. J. Obar, K. M. Khanna, L. Lefrançois, Endogenous naive CD8$^+$ T cell precursor frequency regulates primary and memory responses to infection. *Immunity* **28**, 859–869 (2008). doi: 10.1016/j.immuni.2008.04.010; pmid: 18499487
11. A. Lanzavecchia, F. Sallusto, Understanding the generation and function of memory T cell subsets. *Curr. Opin. Immunol.* **17**, 326–332 (2005). doi: 10.1016/j.coi.2005.04.010; pmid: 15886125
12. F. Sallusto, D. Lenig, R. Förster, M. Lipp, A. Lanzavecchia, Two subsets of memory T lymphocytes with distinct homing potentials and effector functions. *Nature* **401**, 708–712 (1999). doi: 10.1038/44385; pmid: 10537110
13. S. M. Kaech *et al*., Selective expression of the interleukin 7 receptor identifies effector CD8 T cells that give rise to long-lived memory cells. *Nat. Immunol.* **4**, 1191–1198 (2003). doi: 10.1038/ni1009; pmid: 14625547
14. R. M. Kondrack *et al*., Interleukin 7 regulates the survival and generation of memory CD4 cells. *J. Exp. Med.* **198**, 1797–1806 (2003). doi: 10.1084/jem.20030735; pmid: 14662907
15. J. Li, G. Huston, S. L. Swain, IL-7 promotes the transition of CD4 effectors to persistent memory cells. *J. Exp. Med.* **198**, 1807–1815 (2003). doi: 10.1084/jem.20030725; pmid: 14676295
16. J. J. Obar, L. Lefrançois, Memory CD8$^+$ T cell differentiation. *Ann. N. Y. Acad. Sci.* **1183**, 251–266 (2010). doi: 10.1111/j.1749-6632.2009.05126.x; pmid: 20146720
17. J. A. Best *et al*., Transcriptional insights into the CD8$^+$ T cell response to infection and memory T cell formation. *Nat. Immunol.* **14**, 404–412 (2013). doi: 10.1038/ni.2536; pmid: 23396170
18. B. Youngblood, J. S. Hale, R. Ahmed, Memory CD8 T cell transcriptional plasticity. *F1000Prime Rep.* **7**, 38 (2015). doi: 10.12703/P7-38; pmid: 26097712
19. C. M. Carlson *et al*., Kruppel-like factor 2 regulates thymocyte and T-cell migration. *Nature* **442**, 299–302 (2006). doi: 10.1038/nature04882; pmid: 16855590
20. H. Ichii *et al*., Bcl6 is essential for the generation of long-term memory CD4$^+$ T cells. *Int. Immunol.* **19**, 427–433 (2007). doi: 10.1093/intimm/dxm007; pmid: 17307796
21. A. Banerjee *et al*., Cutting edge: The transcription factor eomesodermin enables CD8$^+$ T cells to compete for the memory cell niche. *J. Immunol.* **185**, 4988–4992 (2010). doi: 10.4049/jimmunol.1002042; pmid: 20935204
22. Y. Lou, X. Lu, X. Dang, FOXO1 Up-Regulates Human L-selectin Expression Through Binding to a Consensus FOXO1 Motif. *Gene Regul. Syst. Bio.* **6**, 139–149 (2012). pmid: 23133314
23. B. Kakaradov *et al*., Early transcriptional and epigenetic regulation of CD8$^+$ T cell differentiation revealed by single-cell RNA sequencing. *Nat. Immunol.* **18**, 422–432 (2017). doi: 10.1038/ni.3688; pmid: 28218746
24. M. A. Cannarile *et al*., Transcriptional regulator Id2 mediates CD8$^+$ T cell immunity. *Nat. Immunol.* **7**, 1317–1325 (2006). doi: 10.1038/ni1403; pmid: 17086188
25. F. Masson *et al*., Id2-mediated inhibition of E2A represses memory CD8$^+$ T cell differentiation. *J. Immunol.* **190**, 4585–4594 (2013). doi: 10.4049/jimmunol.1300099; pmid: 23536629
26. B. Hoffman, D. A. Liebermann, Apoptotic signaling by c-MYC. *Oncogene* **27**, 6462–6472 (2008). doi: 10.1038/onc.2008.312; pmid: 18955973
27. O. Cazzalini, A. I. Scovassi, M. Savio, L. A. Stivala, E. Prosperi, Multiple roles of the cell cycle inhibitor p21(CDKN1A) in the DNA damage response. *Mutat. Res.* **704**, 12–20 (2010). doi: 10.1016/j.mrrev.2010.01.009; pmid: 20096807
28. S. M. Kaech, W. Cui, Transcriptional control of effector and memory CD8$^+$ T cell differentiation. *Nat. Rev. Immunol.* **12**, 749–761 (2012). doi: 10.1038/nri3307; pmid: 23080391
29. S. Adutler-Lieber *et al*., Substrate-bound CCL21 and ICAM1 combined with soluble IL-6 collectively augment the expansion of antigen-specific murine CD4$^+$ T cells. *Blood Adv.* **1**, 1016–1030 (2017). doi: 10.1182/bloodadvances.2016001545; pmid: 29296744
30. I. Zaretsky *et al*., Monitoring the dynamics of primary T cell activation and differentiation using long term live cell imaging in microwell arrays. *Lab Chip* **12**, 5007–5015 (2012). doi: 10.1039/c2lc40808b; pmid: 23072772
31. M. Polonsky, B. Chain, N. Friedman, Clonal expansion under the microscope: Studying lymphocyte activation and differentiation using live-cell imaging. *Immunol. Cell Biol.* **94**, 242–249 (2016). doi: 10.1038/icb.2015.104; pmid: 26606974
32. E. D. Hawkins, M. L. Turner, M. R. Dowling, C. van Gend, P. D. Hodgkin, A model of immune regulation as a consequence of randomized lymphocyte division and death times. *Proc. Natl. Acad. Sci. U.S.A.* **104**, 5032–5037 (2007). doi: 10.1073/pnas.0700026104; pmid: 17360353
33. I. Kinjyo *et al*., Real-time tracking of cell cycle progression during CD8$^+$ effector and memory T-cell differentiation. *Nat. Commun.* **6**, 6301 (2015). doi: 10.1038/ncomms7301; pmid: 25709008
34. K. Thurley, D. Gerecht, E. Friedmann, T. Höfer, Three-dimensional gradients of cytokine signaling between T cells. *PLOS Comput. Biol.* **11**, e1004206 (2015). doi: 10.1371/journal.pcbi.1004206; pmid: 25923703
35. Z. Liu *et al*., Immune homeostasis enforced by co-localized effector and regulatory T cells. *Nature* **528**, 225–230 (2015). doi: 10.1038/nature16169; pmid: 26605524
36. N. Waysbort, D. Russ, B. M. Chain, N. Friedman, Coupled IL-2-dependent extracellular feedbacks govern two distinct consecutive phases of CD4 T cell activation. *J. Immunol.* **191**, 5822–5830 (2013). doi: 10.4049/jimmunol.1301575; pmid: 24244020
37. C. A. Sabatos *et al*., A synaptic basis for paracrine interleukin-2 signaling during homotypic T cell interaction. *Immunity* **29**, 238–248 (2008). doi: 10.1016/j.immuni.2008.05.017; pmid: 18674934
38. R. Ahmed, M. J. Bevan, S. L. Reiner, D. T. Fearon, The precursors of memory: Models and controversies. *Nat. Rev. Immunol.* **9**, 662–668 (2009). doi: 10.1038/nri2619; pmid: 19680250
39. A. V. Gett, F. Sallusto, A. Lanzavecchia, J. Geginat, T cell fitness determined by signal strength. *Nat. Immunol.* **4**, 355–360 (2003). doi: 10.1038/ni908; pmid: 12640450
40. M. A. Williams, M. J. Bevan, Shortening the infectious period does not alter expansion of CD8 T cells but diminishes their capacity to differentiate into memory cells. *J. Immunol.* **173**, 6694–6702 (2004). doi: 10.4049/jimmunol.173.11.6694; pmid: 15557161
41. H. Dooms, K. Wolslegel, P. Lin, A. K. Abbas, Interleukin-2 enhances CD4$^+$ T cell memory by promoting the generation of IL-7R α-expressing cells. *J. Exp. Med.* **204**, 547–557 (2007). doi: 10.1084/jem.20062381; pmid: 17312008
42. S. A. Nish *et al*., T cell-intrinsic role of IL-6 signaling in primary and memory responses. *eLife* **3**, e01949 (2014). pmid: 24842874
43. D. M. Mitchell, E. V. Ravkov, M. A. Williams, Distinct roles for IL-2 and IL-15 in the differentiation and survival of CD8$^+$ effector and memory T cells. *J. Immunol.* **184**, 6719–6730 (2010). doi: 10.4049/jimmunol.0904089; pmid: 20483725
44. K. K. McKinstry *et al*., Effector CD4 T-cell transition to memory requires late cognate interactions that induce autocrine IL-2. *Nat. Commun.* **5**, 5377 (2014). doi: 10.1038/ncomms6377; pmid: 25369785
45. D. Comte *et al*., Engagement of SLAMF3 enhances CD4$^+$ T-cell sensitivity to IL-2 and favors regulatory T-cell polarization in systemic lupus erythematosus. *Proc. Natl. Acad. Sci. U.S.A.* **113**, 9321–9326 (2016). doi: 10.1073/pnas.1605081113; pmid: 27482100
46. A. Gérard *et al*., Secondary T cell-T cell synaptic interactions drive the differentiation of protective CD8$^+$ T cells. *Nat. Immunol.* **14**, 356–363 (2013). doi: 10.1038/ni.2547; pmid: 23475183
47. F. Zhao, J. L. Cannons, M. Dutta, G. M. Griffiths, P. L. Schwartzberg, Positive and negative signaling through SLAM receptors regulate synapse organization and thresholds of cytolysis. *Immunity* **36**, 1003–1016 (2012). doi: 10.1016/j.immuni.2012.05.017; pmid: 22683123
48. O. Feinerman *et al*., Single-cell quantification of IL-2 response by effector and regulatory T cells reveals critical plasticity in immune response. *Mol. Syst. Biol.* **6**, 437 (2010). doi: 10.1038/msb.2010.90; pmid: 21119631
49. D. A. Jaitin *et al*., Massively parallel single-cell RNA-seq for marker-free decomposition of tissues into cell types. *Science* **343**, 776–779 (2014). doi: 10.1126/science.1247651; pmid: 24531970

ACKNOWLEDGMENTS

We thank I. Shachar and L. Radomir for help with *Slamf6*$^{-/-}$ mice and useful discussions, and R. Alon and S. Feigelson for help with ICAM-1 coating protocol and productive conversations. We also thank T. Bigdari for the design of the graphical abstract and N. David for help with figure design. **Funding:** N.F. was supported by the Israel Science Foundation (grant no. 1184/15) and by a grant from the Israel Ministry of Science, Technology and Space and the German Cancer Research Center (DKFZ). N.F. is Incumbent of The Eugene and Marcia Appelbaum Professorial Chair.

N.F. and B.C. were supported by a grant from the Weizmann UK foundation. B.C. is supported by a Weston Visiting Professorship from the Weizmann Institute of Science.
Author contributions: M.P. was involved in the design and implementation of all experiments and computer simulations, performed downstream and statistical analysis, generated the figures, and wrote the manuscript. J.R. was involved in implementation of image analysis algorithms and provided initial insights for this study. A.K.P. constructed the stochastic simulations. I.Z. conducted adoptive transfer experiments. S.M conducted quantitative PCR experiments. C.B constructed cDNA libraries and conducted RNA-seq. E.D, N.K., and G.S. were involved in downstream analysis of RNA-seq. data. Z.P. conducted image-stream analysis. B.C and N.F designed experiments, supervised all stages of the project, and wrote the manuscript. **Competing interests:** The authors declare no competing interests **Data and materials availability:** MATLAB code used for single-cell stochastic simulations, including additional parameters that are required for the run, can be downloaded through GitHub: https://github.com/innate2adaptive/Single-cell-imaging. RNA-seq data have been deposited to Gene Expression Omnibus (GEO) with the accession no. GSE112347. All other data needed to evaluate the conclusions in this paper are present either in the main text or the supplementary materials.

SUPPLEMENTARY MATERIALS

www.sciencemag.org/content/360/6394/eaaj1853/suppl/DC1
Supplementary Text
Figs. S1 to S16
Tables S1 to S5
Movie S1
References (*50*–*52*)

9 September 2016; resubmitted 19 December 2017
Accepted 17 April 2018
10.1126/science.aaj1853

Science

Induction of CD4 T cell memory by local cellular collectivity

Michal Polonsky, Jacob Rimer, Amos Kern-Perets, Irina Zaretsky, Stav Miller, Chamutal Bornstein, Eyal David, Naama Meira Kopelman, Gil Stelzer, Ziv Porat, Benjamin Chain and Nir Friedman

Science **360** (6394), eaaj1853.
DOI: 10.1126/science.aaj1853

Modeling memory differentiation in T cells

The balance between effector and central memory T cells shifts toward the latter as the number of T cells participating in immune responses increases. Polonsky *et al.* determined the mechanisms by which T cell quorum sensing affects memory differentiation by using live-cell imaging to track cell proliferation and differentiation. They found that the rate of memory $CD4^+$ T cell differentiation is determined by cell number. This rate substantially increases above a threshold number of locally interacting cells. Mathematical modeling suggests that the number of initially seeded cells and the number of cell divisions are not critical. Instead, the instantaneous number of interacting cells continuously modulates the differentiation rate. This is partly fueled by increased sensitivity to the cytokines interleukin-2 (IL-2) and IL-6, independent of any effects on cell proliferation.

Science, this issue p. eaaj1853